

Principles of Dielectric Blood Coagulometry as a Comprehensive Coagulation Test

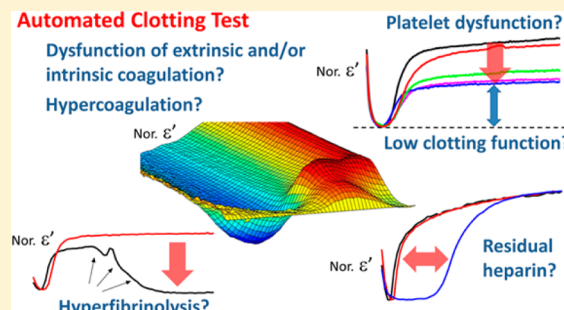
Yoshihito Hayashi,*[†] Marc-Aurèle Brun,[†] Kenzo Machida,[†] and Masayuki Nagasawa[‡]

[†]LOC Development Department, R&D Division, Medical Business Unit, Sony Corporation, in Tokyo Medical and Dental University, 1-5-45 Yushima Bunkyo-ku, Tokyo 113-8510, Japan

[‡]Department of Pediatrics, Tokyo Medical and Dental University, 1-5-45 Yushima Bunkyo-ku, Tokyo 113-8510, Japan

Supporting Information

ABSTRACT: Dielectric blood coagulometry (DBCM) is intended to support hemostasis management by providing comprehensive information on blood coagulation from automated, time-dependent measurements of whole blood dielectric spectra. We discuss the relationship between the series of blood coagulation reactions, especially the aggregation and deformation of erythrocytes, and the dielectric response with the help of clot structure electron microscope observations. Dielectric response to the spontaneous coagulation after recalcification presented three distinct phases that correspond to (P1) rouleau formation before the onset of clotting, (P2) erythrocyte aggregation and reconstitution of aggregates accompanying early fibrin formation, and (P3) erythrocyte shape transformation and/or structure changes within aggregates after the stable fibrin network is formed and platelet contraction occurs. Disappearance of the second phase was observed upon addition of tissue factor and ellagic acid for activation of extrinsic and intrinsic pathways, respectively, which is attributable to accelerated thrombin generation. A series of control experiments revealed that the amplitude and/or quickness of dielectric response reflect platelet function, fibrin polymerization, fibrinolysis activity, and heparin activity. Therefore, DBCM sensitively measures blood coagulation via erythrocytes aggregation and shape changes and their impact on the dielectric permittivity, making possible the development of the battery of assays needed for comprehensive coagulation testing.



The dependence of warfarin efficacy on diet and other drugs and consequent need for regular monitoring of prothrombin time international normalized ratio (PT-INR) is an example of therapeutic drug monitoring to avoid bleeding events in thrombosis patients.^{1,2} The introduction of new anticoagulant drugs in recent years and reports of associated bleeding events,^{3–5} as well as the lack of standardized testing to monitor antiplatelet therapies,^{1,6–8} foster a need for the development of comprehensive hemostasis testing.

Also, during the perioperative period, comprehensive hemostasis monitoring is required because appropriate treatment may differ if hemostatic imbalance is caused by surgical invasiveness or by clotting and/or platelet dysfunction.^{9–13} Such monitoring provides the evidence for transfusion and helps reduce unnecessary use of blood products and associated infection risks.¹⁴

Widely used methods for hemostasis testing are PT-INR and activated partial thromboplastin time (aPTT)¹⁵ and, for heparin dosage control, activated coagulation time (ACT).¹⁶ Because of the use of coagulation initiators in large excess, such methods mainly test bleeding tendency and have limited sensitivity to hypercoagulation.^{17,18} Moreover, because information on platelet function, thrombus strength, and fibrinolytic system is

not available,^{11,15} the test results may not properly reflect the actual *in vivo* condition.

Thrombelastography/thromboelastometry measures viscoelastic changes during blood coagulation, providing comprehensive information through a combination of multiple assays.^{11,19} Thromboelastometry has been used to provide evidence for transfusion in major surgeries and was reported to contribute to medical expenses reduction.¹⁴ It has been pointed out, however, that stress and distortion during measurements are not controlled in those methods, so that measures themselves affect clot formation, interfering with the proper determination of clotting time (CT) and clot strength.²⁰

We previously compared dielectric spectroscopy and rheological measurements of blood coagulation.²¹ The time-dependent dielectric permittivity at 760 kHz exhibited a characteristic peak whose position shifted to shorter times with increasing thrombin concentration and agreed well with the start of coagulation determined using a damped oscillation rheometer.²² However, this was a preliminary report and we did

Received: July 20, 2015

Accepted: September 14, 2015

Published: September 14, 2015

Table 1. Materials

material code ^a	name of material/product	manufacturer	preparation/note
A	blood collection tube for coagulation testing	Nipro Corp.	amount of blood collection: 1.8 mL (mixed in a ratio of 9:1 with 3.13% citric acid)
B	calcium chloride solution (1 M)	Sigma-Aldrich	diluted by distilled water to 200 mM
C	urokinase from human kidney cells	same as above	dissolved in distilled water (50 000 units/mL) and further diluted 10-fold with PBS (5000 units/mL)
D	heparinase I from <i>Flavobacterium heparinum</i>	same as above	dissolved in PBS (500 units/mL); then, a solution of 95 units/mL heparinase I and 200 mM CaCl ₂ was prepared with 1 M CaCl ₂ solution and distilled water
E	dade inovin (reagent for PT test; tissue factor)	Sysmex Corp.	dissolved in 4 mL of distilled water according to the instruction from the manufacturer; this stock solution was diluted 100 times in distilled water and further diluted 6 times in PBS for use
F	actin FSL (reagent for aPTT test; ellagic acid)	same as above	diluted 6-fold with PBS
G	cytochalasin D	Wako Pure Chemical Industries	dissolved in DMSO to 2000 µg/mL; distilled water and HEPES buffer was then added to make a solution of 165 µM cytochalasin D in 20 mM HEPES solution
H	tissue plasminogen activator from human melanoma cell (tPA)	same as above	dissolved in distilled water to prepare a solution of 60 000 units/mL and further diluted 10-fold with PBS (6000 units/mL)
I	aprotinin from bovine lung	same as above	dissolved using PBS and 1 M CaCl ₂ ; a solution of 6800 k units/mL and 200 mM CaCl ₂ was prepared
J	DMSO	same as above	used to solve cytochalasin D
K	PBS	same as above	used for preparation of the reagents
L	synthetic peptide H-Gly-Pro-Arg-Pro-OH (Pefabloc FG)	Pentapharm	dissolved in physiological saline (100 mg/mL)
M	HEPES buffer (1 M)	Dojindo Laboratories	used in preparation of the cytochalasin D solution
N	physiological saline	Otsuka Pharmaceutical	used both to adjust the dilution rate of blood samples and to solve H-Gly-Pro-Arg-Pro-OH
O	hepaflush 10 units/mL (heparin sodium)	Terumo Corp.	used as received

^aReferred to in Table 2.

Table 2. Conditions of Verification Experiments for DBCM

test no.	type of test	modification of sample blood	reagent (quantity)	used materials*
T0	rouleau formation	as collected	none	A
T1	spontaneous clotting	as collected	200 mM calcium solution (12 µL)	A, B
T2	extrinsic activation	as collected	diluted dade inovin tissue factor solution (12 µL) + 200 mM calcium solution (12 µL)	A, B, E(K)
T3	platelet inhibition	addition of cytochalasin D (final concentrations: 0, 3.6, 5.0, and 10 µM); the dilution rate of blood was kept the same at 0.935 using physiological saline	same as above	A, B, E(K), G(J, M), N
T4	fibrin polymerization inhibition	addition of H-Gly-Pro-Arg-Pro-OH (final concentration: 0, 0.5, 1.0, and 2.0 mg/mL); the dilution rate of blood was kept the same at 0.917 using physiological saline	same as above	A, B, E(K), L(N), N
T5	fibrinolytic response	addition of tPA or urokinase solution at a total blood dilution rate of 0.962	same as above	A, B, E, H(K) or C(K)
T6	fibrinolysis inhibition	same as above	diluted dade inovin tissue factor solution (12 µL) + aprotinin solution (12 µL)	A, E, I(B), H(K), or C(K)
T7	intrinsic activation	as collected	diluted actin FSL ellagic acid solution (12 µL) + 200 mM calcium solution (12 µL)	A, B, F(K)
T8	heparin effect	addition of Hepaflush at a total blood dilution rate of 0.909	same as above	A, B, F(K), O
T9	heparin neutralization	same as above	diluted actin FSL ellagic acid solution (12 µL) + heparinase solution (12 µL)	A, B, F(K), D(B, K), O

*See material codes in Table 1.

not have a clear overall picture of the mechanisms underlying the changes in the permittivity spectrum as blood coagulates.

Although dielectric spectroscopy is not a particularly common measurement method in the medical field, pioneering research goes back to Debye in the first half of the 20th century,²³ followed by Grant et al.,²⁴ Foster and Schwan,²⁵ Pethig,²⁶ Takashima,²⁷ Asami,²⁸ Feldman et al.,²⁹ and many

others³⁰ who performed research on the physical properties of biological molecules and cells. The main dielectric response from blood in the MHz range is known to be from cell membrane interfacial polarization²⁹ that changes substantially with cell shape and aggregation³¹ including rouleau formation of erythrocytes.^{32,33} Because erythrocytes incorporation in the fibrin network³⁴ and further clot retraction due to the action of

platelets³⁵ incur erythrocyte shape modification that is visible on clots scanning electron microscope (SEM) images,³⁴ the main dielectric response is likely to change during coagulation. On the other hand, the huge artificial dielectric response in the kHz and lower ranges due to electrode polarization is usually observed for ionic samples including blood.^{29,36,37}

In the present study, nonclinical research was conducted using a prototype apparatus to clarify the principles of dielectric blood coagulometry (DBCM). The results of dielectric spectroscopy measurements are discussed in comparison with a model of erythrocyte aggregation/transformation accompanying blood coagulation. In advancing such discussion, SEM and transmission electron microscopy (TEM) observation of the fibrin network and erythrocytes status on the surface and inner portions of clots provided valuable insights. In addition, the DBCM responses to coagulation in the presence of various activators or inhibitors were examined to show that DBCM can assess platelet function, fibrin formation, fibrinolysis, and anticoagulant effect of heparin.

EXPERIMENTAL SECTION

Sample Blood and Reagents. This study was approved by the Ethics Committee of Tokyo Medical and Dental University. Blood samples were drawn into collection tubes with sodium citrate from four healthy volunteers who consented to the study. The reagents and their preparation are listed in Table 1.

Dielectric Blood Coagulometry. Dielectric measurements were done using an automated blood coagulation analyzer prototype (Sony Corporation). The measurement temperature was 37 °C, and the measurement frequency range covered 100 Hz to 10 MHz. A whole blood sample of 180 μL was dispensed into a polypropylene disposable cartridge with titanium electrodes inserts, mixed and stirred with the reagents previously pipetted into the cartridge. Measurements started immediately, and the dielectric spectrum of the sample was recorded over time. To minimize artifacts from erythrocyte sedimentation, cartridges were designed so that the sedimentation boundary would not reach the top of electrodes height during measurements (Figure S1). Table 2 summarizes the experimental conditions, identified by test numbers T0 to T9, used to verify the responses to rouleau formation without clotting (T0), spontaneous clot formation (T1), extrinsic activation (T2), platelet inhibition by cytochalasin D (CyD) (T3),^{38–40} fibrin polymerization inhibition by H-Gly-Pro-Arg-Pro-OH (T4),^{38,41,42} fibrinolytic response and fibrinolysis inhibition (T5 and T6), and intrinsic activation, heparin effect, and heparin neutralization (T7, T8, and T9).

Dielectric Measurements of the Rouleau Formation Process (T0). The change in permittivity accompanying rouleau formation in citrated whole blood was observed without recalcification, so that coagulation did not occur. Specimen blood dispensed into the cartridge was agitated by manual pipetting movements. Measurements started within 5 s after agitation ended, and changes in the dielectric spectrum were recorded over time. After approximately 10 min, blood in the cartridge was agitated again, and the dielectric measurement was restarted. The above actions were repeated to confirm both reproducibility and reversibility.

SEM and TEM Measurements. After DBCM measurements, samples were processed for SEM and TEM observation. The series of procedures for preparing samples followed general methods. First, each disposable cartridge was cut in two with a razor and left in that state for fixation with 2.5%

glutaraldehyde in PBS for 2 h at room temperature. The specimens were washed overnight at 4 °C in the same buffer and postfixed with 1% OsO₄ buffered with 0.1 M PBS for 2 h. The specimens were dehydrated in a graded series of ethanol. During this work, clots were completely removed from the severed cartridges in the 90% ethanol stage. Next, SEM samples were dried in a critical point drying apparatus (HCP-2: Hitachi) with liquid CO₂. The specimens were sputter-coated with platinum and examined using a SEM (S-4500: Hitachi). The samples for TEM were embedded in Epon 812. Semithin sections were cut at 1 μm and stained with toluidine blue. Ultrathin sections, 90 nm, were collected on copper grids, double-stained with uranyl acetate and lead citrate, and then observed using a TEM (H-7100: Hitachi).

RESULTS

Spontaneous Clotting (T1) and Rouleau Formation (T0). Permittivity of blood changed dynamically with blood coagulation. The typical result is shown in the plot of normalized permittivity as a function of time and frequency in Figure 1a. Among that data, the permittivity at 10 MHz

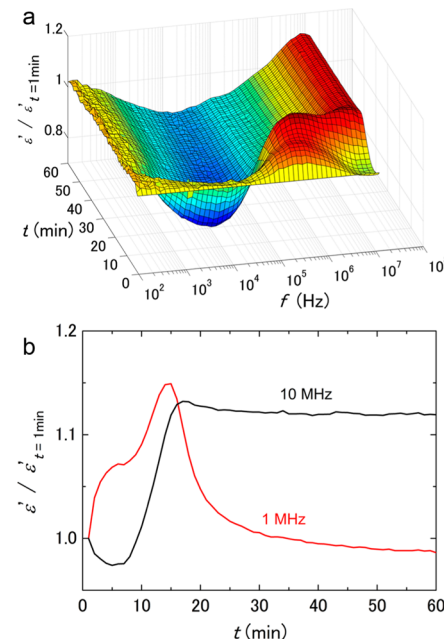


Figure 1. Typical DBCM response of spontaneous blood coagulation. The changes in permittivity that occur with coagulation are normalized by data 1 min after recalcification. Panel (a) is a 3D image showing the changes in all measured frequencies. Characteristic changes are visible in the MHz band, corresponding to erythrocytes interfacial polarization. Panel (b) is an extract from panel (a) showing the changes at 1 and 10 MHz. At 1 MHz, a two-step peak is observed, but at 10 MHz, the value reaches a minimum at an early stage before increasing to an almost constant value.

passes through a shallow minimum in the early stage and then increases until it reaches a nearly constant value, while at 1 MHz, there are two local maxima and a subsequent decrease (Figure 1b). Microscopic observation of blood suggested that the decrease at 10 MHz and increase at 1 MHz soon after the start of the measurement are due to rouleau formation (Figure S2). This was confirmed by the dielectric measurements of blood under the anticoagulation state as shown in Figure 2,

where the reversibility of rouleau formation is reflected by the permittivity changes induced by agitation.

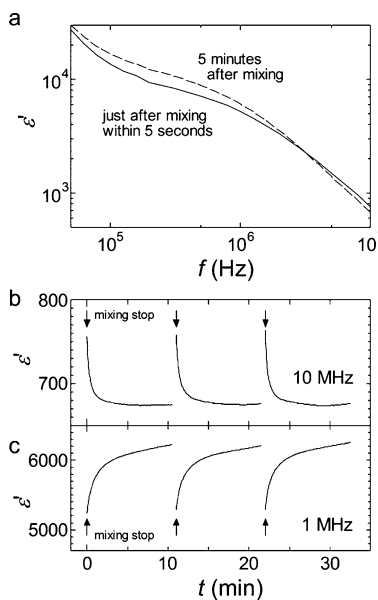


Figure 2. Rouleau formation and dielectric response. Panel (a) shows the dielectric spectrum right after pipet mixing and 5 min after mixing stopped. Panels (b) and (c) show the dielectric changes at 10 and 1 MHz, respectively. These changes were measured as mixing was stopped and started again, three times in a row. The arrows indicate the point at which mixing was stopped.

Observations with SEM/TEM. The SEM images in Figure 3a–c show that the clot surface is covered with a dense fibrin network. Cines et al.³⁴ reported similar images but with less dense networks probably because of the different experimental conditions. These images indicate that erythrocytes clumped together in a fibrin network change shape and become polyhedrocytes as a result of the large compressive force from platelet clot retraction. In our SEM images, on the other hand, only a limited degree of shape transformation is observed, probably because the erythrocytes located near fissures in the clot suffer from reduced compressive force. Indeed, TEM images (Figure 3d) show that many cell cross sections are not consistent with normal erythrocyte shape, suggesting erythrocyte aggregation and shape modification in the central portion of clots. We note that TEM images of clots in the presence of a platelet inhibitor show less erythrocytes aggregation and transformation (Figure S3).

Effects of Blood Coagulation/Fibrinolysis Activators and Inhibitors (T2 to T6). The permittivity curves at 10 and 1 MHz for extrinsic activation (T2) and spontaneous clotting (T1) assays are compared in Figure 4a,b, respectively. At 10 MHz, the curve shifted toward shorter times upon activation, while the curve shape changed at 1 MHz.

Figure 5a shows the extrinsic activation curves (10 MHz) at different CyD concentrations corresponding to different platelet function levels (T3). The amplitude from the minimum value decreased with increasing CyD concentrations and leveled off above 5 μM . This convergence was similarly observed in a thromboelastography study.³⁸ On the other hand, no significant change in the minimum position was observed. As discussed later, this is consistent with the fact that CyD does not affect thrombin production and fibrin polymerization.

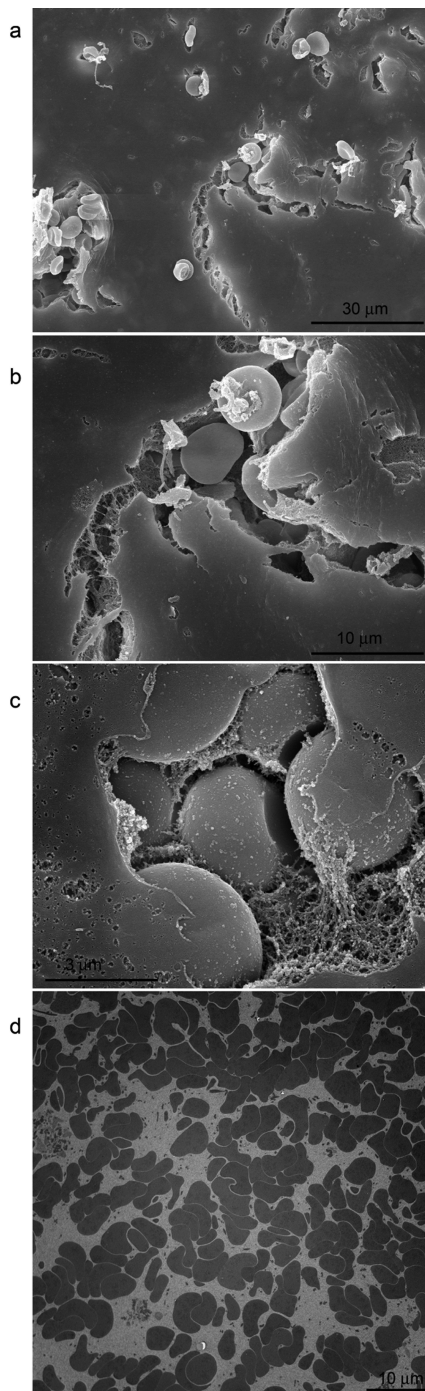


Figure 3. SEM and TEM images of a clot. On the SEM image, the clot surface covered with fibrin is observed as well as erythrocytes seen through surface fissures (a, b, c). On the TEM image, erythrocytes that are clumped together and have deformed shapes are visible in the clot interior (d).

Corresponding data at 1 MHz are shown in Figure S4 as a typical example of the clot strength influence at this frequency.

Different fibrin polymerization levels were reproduced in vitro by varying H-Gly-Pro-Arg-Pro-OH concentration (T4) in an extrinsic activation assay. Figure 5b shows that the amplitude and rate of the increase from the minimum value decreased with increasing concentrations of H-Gly-Pro-Arg-Pro-OH. No significant prolongation of the time corresponding to the minimum value was observed below 1.0 mg/mL. This agrees

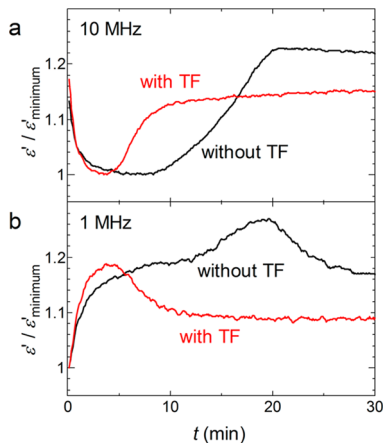


Figure 4. Results of extrinsic activation. The changes at 10 MHz (a) and 1 MHz (b) are shown using permittivity normalized by the minimum value and compared with samples without tissue factor.

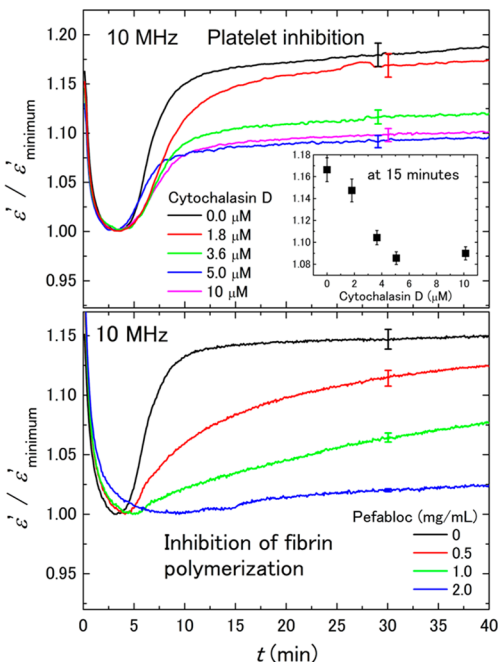


Figure 5. Changes due to platelet or fibrin polymerization inhibition. The changes in permittivity at 10 MHz normalized by the minimum value are shown with error bars indicating levels of uncertainty due to the normalization by the minimum values. (a) The amplitude diminution as cytochalasin D concentration increases is visible. In the inset, the normalized permittivity 15 min after the start of measurements is plotted against cytochalasin D concentration. (b) The amplitude diminution as the fibrin polymerization inhibitor concentration increases is visible.

with the argument of Chakroun et al.³⁸ that, though H-Gly-Pro-Arg-Pro-OH inhibits fibrin polymerization, it has almost no effect on the upstream of blood coagulation cascade, before thrombin production is started.

Figure 6a,b shows the extrinsic activation curves with the addition of tissue plasminogen activator (tPA) and urokinase, respectively (T5), as well as the results of fibrinolysis inhibition by aprotinin (T6). In the absence of aprotinin, the permittivity at 10 MHz first increased with clot formation, then settled at a constant value, and finally decreased as fibrinolysis settled in. When fibrinolysis is inhibited by aprotinin, the final decrease

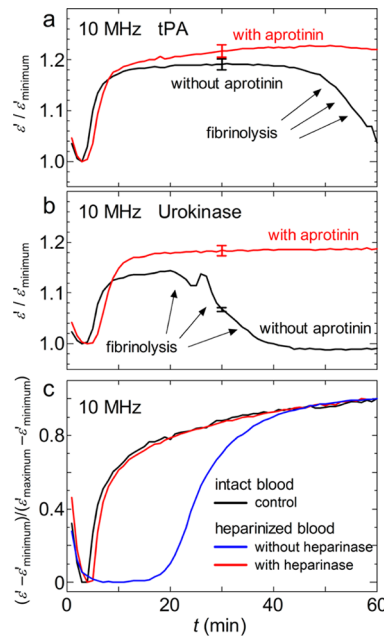


Figure 6. Responses to fibrinolysis activation and residual heparin. The changes in permittivity at 10 MHz normalized by the minimum value are shown in panels (a) and (b) with error bars indicating levels of uncertainty due to the normalization by the minimum value. The sample of panels (a) and (b) are made by addition of tPA and urokinase to the blood specimen, respectively. Responses in the presence and absence of a fibrinolysis inhibitor (aprotinin) are shown. The experiment using tPA (a) and urokinase (b) were carried out using specimens from separate healthy people. In panel (c), the changes in permittivity at 10 MHz normalized by both the minimum value and the value 60 min after the start of measurements are shown. Upon heparin addition to the blood specimen, a significant delay in the response was observed in comparison with intact blood. This delay disappeared with the neutralization of heparin by heparinase, and a response similar to that of intact blood was observed.

disappeared. This demonstrates that with DBCM it is possible to observe thrombolysis as a decrease in permittivity at 10 MHz after clot formation. We note that fibrinolysis induced changes at 1 MHz, as well (Figure S5).

The contribution of heparin is generally observed as an extension of the coagulation onset time of the intrinsic activation assay (T7).¹⁴ Figure 6c shows that the DBCM response was prolonged due to the addition of heparin (T8) and that this prolongation was lost upon heparin neutralization with the addition of heparinase (T9). Figure S6 shows the corresponding results at 1 MHz.

DISCUSSION

Analysis of Dielectric Spectra. A dielectric spectrum is modeled by a function, appropriately chosen to represent the physical mechanism behind the spectrum, which contains, among others, relaxation strength $\Delta\epsilon$ and frequency f_c (see Figure 7a,b for definition) as fitting parameters.^{27–29,31,36} Following well-established dielectric spectroscopy theory of cell suspensions, we assumed a Cole–Cole function and a constant phase angle impedance to model erythrocytes interfacial polarization and electrode polarization, respectively. The curved lines in Figure 7a,b are the best-fit results to the actual data, while the broken lines show only the relevant contribution from erythrocytes. Changes of $\Delta\epsilon$ and f_c with

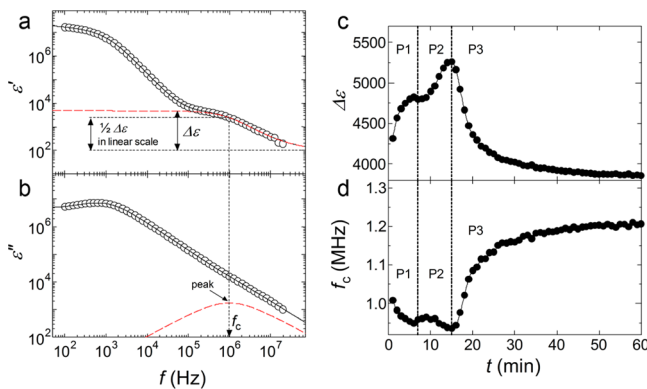


Figure 7. Dielectric relaxation analysis and blood coagulation phase identification. Panel (a) shows the real part and panel (b) the imaginary part of the complex permittivity. The broken red lines are the result of an analysis of the interfacial polarization phenomenon according to a Cole–Cole type dielectric relaxation function. This function is characterized by the relaxation strength $\Delta\epsilon$ corresponding to changes in ϵ' (a) and the relaxation frequency f_c that corresponds to the peak of this function observed in the imaginary part of permittivity, ϵ'' (b). The curved lines in the figure are the sum of all the assumed contributions in the analysis, and agree well with the experimental values. Spontaneous whole blood coagulation data shown in Figure 1 were analyzed using a Cole–Cole type dielectric relaxation modeling. The changes in relaxation strength and relaxation frequency are shown in panel (c) and (d), respectively. In P1, immediately after the start of measurements the response to rouleau formation is observed. It is followed by the response to blood coagulation induced erythrocyte aggregation in the P2 phase and the response to erythrocytes deformation corresponding to clot retraction in the P3 phase.

proceeding spontaneous clotting (T1) are shown in Figure 7c,d.

Here, we would like to review the relationship between data at 1 or 10 MHz presented in Figures 2b,c, and 4–6 and the dielectric relaxation parameters $\Delta\epsilon$ and f_c . In a dielectric measurement of whole blood, permittivity at 1 MHz is sensitive to $\Delta\epsilon$ changes and less sensitive to shifts of f_c . In comparison, permittivity at 10 MHz is sensitive to both $\Delta\epsilon$ changes and small shifts of f_c . For a numerical example using the Cole–Cole function presented in Figure 7a, a 20% increase of $\Delta\epsilon$ induces 19% and 15% increases of the permittivity at 1 and 10 MHz, respectively, while a 20% increase of f_c induces 10% and 14% increases at those frequencies. Therefore, monitoring of 1 and 10 MHz allows us to access information about $\Delta\epsilon$ and f_c changes with blood coagulation. To realize DBCM as a medical device, data analysis using specific frequencies is easier to implement than nonlinear curve fitting and suitable for an automated system.

Phase 1: Rouleau Formation Process. The results of rouleau formation measurements presented in Figure 2 suggest that the initial increase in $\Delta\epsilon$ and decrease in f_c for several minutes after the start of measurements in Figure 7c,d, hereafter referred to as phase 1 (P1), are attributable to the rouleau formation process. Referring to past reports,^{43,44} we suppose that P1 covers the whole stepwise rouleau formation process and regroups linear erythrocyte aggregation spanning several seconds, incorporation of aggregates in a three-dimensional network during several minutes, and final transformation into spherical aggregates.

Phase 2: Erythrocytes Aggregation Occurring with Coagulation. Whole blood recalcification time was manually measured (Figure S7). The time until blood loses its fluidity,

CT, was determined visually as $CT = 330 \pm 30$ s and was found to agree with the start of phase 2 (P2) in Figure 7c,d. P2 is characterized by the increase of $\Delta\epsilon$ and minimal changes in f_c observed approximately 7 min from the start. The fact that the coagulation-induced DBCM response starts from CT is consistent with reports by Chernysh et al.^{45,46} that fibrin network formation continues after CT and a report by Rand et al.⁴⁷ that no more than 2% of prothrombin had become α -thrombin and, moreover, that only approximately 15% of it was acting on fibrinogen at CT. During P2, therefore, it is reasonable to assume that erythrocytes move with considerable freedom so that they continue to form aggregates trapped in fibrin networks.³⁴ We think that the original rouleau structure is conserved while further aggregation proceeds during the early phase of coagulation, which is in line with arguments suggesting the production of soluble fibrin polymers is the main force promoting aggregation in this phase.^{48,49} There may also be an increase in heterogeneity from the rearrangement of the aggregate structures. From a numerical simulation based on the dielectric response theory of heterogeneous systems, the permittivity near 1 MHz was reported to increase with cell aggregation.²¹ Even when the aggregation level is assumed constant, the permittivity near 1 MHz would increase when hollow (foam-structured) elements are formed from the rearrangement of the aggregate structures. Almost no change in f_c was observed in that theoretical analysis.²¹ These observations appear coherent with the behaviors of $\Delta\epsilon$ and f_c observed in P2.

Phase 3: Change in Erythrocyte Shape with Blood Coagulation.

Phase 3 (P3) in Figure 7c,d is characterized by the decrease in $\Delta\epsilon$ and increase in f_c approximately 15 min from the start. Both a SEM study by Cines et al.³⁴ and our TEM images (Figure 3d) demonstrate the shape transformation of erythrocytes from native discocytes to polyhedral erythrocytes during clot formation. A systematic study of the influence of erythrocytes shape on the dielectric spectra has demonstrated that, at constant volume fraction, $\Delta\epsilon$ decreases while f_c increases as the native shape is transformed into other shapes (Figures S8 and S9).³¹ It is possible that, in addition to this, the partial disappearance of the rouleau structure within aggregates also contributes to the observed changes. A careful observation of TEM images (Figure 3d) indeed suggests that rouleau structures after coagulation appear disturbed compared to noncoagulated blood observed using an optical microscope (Figure S2).

Effects from Blood Coagulation Activators. As shown in Figure 4, in assays accelerated by tissue factor, not only does the response time shorten but also the amplitude and shape of the change (especially 1 MHz, Figure 4b) differ in comparison with spontaneous coagulation. Such behavior was repeatedly observed for different individuals (data not shown). Therefore, it seems to be the general response to activation of blood coagulation. This is thought to be because the response deemed to be the erythrocyte aggregation phase (P2) that accompanies blood coagulation shown in Figure 7c,d shifts before it can proceed to the next phase (the erythrocyte deformation that occurs with blood coagulation, P3). Visually determined $CT = 165 \pm 15$ s in the presence of tissue factor was found to agree with the time corresponding to a permittivity minimum at 10 MHz. Ninivaggi et al.⁵⁰ developed a whole blood thrombin production assay and reported thrombin production lag times of 4.8 and 4.2 min at tissue factor concentrations of 0.5 and 1.0 pM, respectively, and thrombin production maximum at 6.9

and 6.3 min, respectively. Because the final concentration of tissue factors in our extrinsic activation assay was 0.6–0.7 pM, within the above test concentrations, the start of P3 at 4 min and the maximal increase rate at 6 min are seen to be coherent with the time scale reported by Ninivaggi et al.⁵⁰

Platelet inhibition adversely affects clot retraction and thus limits erythrocyte deformation and disturbance of rouleau structures within aggregates, so that the amplitude of P3 diminishes with increasing inhibitor concentration, as shown in Figure 5a. Yet, the stagnation of P3 amplitude with excess inhibitor concentrations suggests that erythrocyte deformation and aggregates disappearance occur, though in a limited way, even under platelet total inhibition. Conversely, when fibrin formation is inhibited significantly, it appears that almost no erythrocyte deformation occurs even when there is no effect on platelet activity (Figure 5b). This agrees with the fact that clot retraction does not occur unless fibrin networks are formed.

Fibrinolytic System Monitoring and Evaluation of Residual Heparin. In the clot lysis process, the dielectric response approaches the value before blood coagulation (Figure 6a,b). This is thought to be because erythrocytes recover their native shape as the clot compressive force is relaxed with the loss of the fibrin network.

Heparin remaining in blood forms complexes with antithrombin III and effectively inhibits thrombin, producing a delay in the blood coagulation reaction (Figure 6c). When heparinase is added, this delay disappears. Thus, it is possible to determine whether the reason for the coagulation delay is due to residual heparin or to other coagulation abnormalities by comparing measurement results under the two conditions, with and without heparinase.

CONCLUSIONS

For effective thrombosis and hemostasis treatment in the perioperative period, a comprehensive test that can evaluate the coagulation and fibrinolytic capacity of whole blood samples simply and quantitatively is effective. In the field of internal medicine as well, there are clear needs in the management of new anticoagulant therapies using direct thrombin inhibitors or factor Xa inhibitors. DBCM meets these needs by sensitively measuring and analyzing changes in permittivity with blood coagulation. The main dielectric response on DBCM is produced by the aggregation and shape transformation of erythrocytes during coagulation. This response was useful to evaluate the activation of the extrinsic and intrinsic blood coagulation reaction pathways. Decreases in the amount of change were also observed to be dependent on the concentration of platelet inhibitors and fibrin aggregation inhibitors. Examples of measurements were also shown for fibrinolysis activity and residual heparin evaluation, which are important as perioperative tests. According to these results, proofs of concept for multiple assays have been established to realize comprehensive coagulation testing with an automated point-of-care device. Further evaluation of DBCM is now ongoing through clinical studies to statistically demonstrate the reliability of the multiple parameters quantitatively extracted from the dielectric response, such as CT, the clotting amplitude, and clotting velocity. It is a new blood coagulation test method that is promising for the achievement of personalized medicine in the coming years.

ASSOCIATED CONTENT

Supporting Information

The Supporting Information is available free of charge on the ACS Publications website at DOI: [10.1021/acs.analchem.5b02723](https://doi.org/10.1021/acs.analchem.5b02723).

Diagram of the disposable cartridge, optical microscope and TEM images, and other data ([PDF](#))

AUTHOR INFORMATION

Corresponding Author

*Tel.: +81 3 3811 8970. Fax: +81 3 5803 4790. E-mail: Yoshihito.Hayashi@jp.sony.com.

Notes

The authors declare the following competing financial interest(s): Y.H., M.-A.B. and K.M. are employees of Sony Corp. M.N. declares no competing financial interests.

ACKNOWLEDGMENTS

This work was partially supported by the Medical Research and Development Programs Focused on Technology Transfer: Development of Advanced Measurement and Analysis Systems (SENTAN) from Japan Agency for Medical Research and Development, AMED (Y.H.). A part of this study for SEM and TEM observations was supported by the Project at Tokyo Medical and Dental University for Creation of Research Platforms and Sharing of Advanced Research Infrastructure of the Ministry of Education, Culture, Sports, Science and Technology of Japan. We would like to thank Ms. Aya Murata, Ms. Seungmin Lee, and Ms. Kaori Kawaguchi, from Sony Corp., for their helpful discussion.

REFERENCES

- (1) Marder, V. J.; Aird, W. C.; Bennett, J. S.; Schulman, S.; White, G. C., Eds. *Hemostasis and Thrombosis: Basic Principles and Clinical Practice*, 6th ed.; Lippincott Williams & Wilkins: Philadelphia, 2013.
- (2) Greenblatt, D. J.; von Moltke, L. L. *J. Clin. Pharmacol.* **2005**, *45*, 127–132.
- (3) Connolly, S. J.; Ezekowitz, M. D.; Yusuf, S.; Eikelboom, J.; Oldgren, J.; Parekh, A.; Pogue, J.; Reilly, P. A.; Themelis, E.; Varrone, J.; Wang, S.; Alings, M.; Xavier, D.; Zhu, J.; Diaz, R.; Lewis, B. S.; Darius, H.; Diener, H. C.; Joyner, C. D.; Wallentin, L. N. *Engl. J. Med.* **2009**, *361*, 1139–1151.
- (4) EINSTEIN Investigators; Bauersachs, R.; Berkowitz, S. D.; Brenner, B.; Buller, H. R.; Decousus, H.; Gallus, A. S.; Lensing, A. W.; Misselwitz, F.; Prins, M. H.; Raskob, G. E.; Segers, A.; Verhamme, P.; Wells, P.; Agnelli, G.; Bounnameaux, H.; Cohen, A.; Davidson, B. L.; Piovella, F.; Schellong, S. N. *Engl. J. Med.* **2010**, *363*, 2499–2510.
- (5) Patel, M. R.; Mahaffey, K. W.; Garg, J.; Pan, G.; Singer, D. E.; Hacke, W.; Breithardt, G.; Halperin, J. L.; Hankey, G. J.; Piccini, J. P.; Becker, R. C.; Nessel, C. C.; Paolini, J. F.; Berkowitz, S. D.; Fox, K. A.; Califff, R. M. N. *Engl. J. Med.* **2011**, *365*, 883–891.
- (6) Gachet, C.; Aleil, B. *Eur. Heart J. Suppl.* **2008**, *10*, A28–A34.
- (7) Lenk, E.; Spannagl, M. *J. Int. Fed. Clin. Chem.* **2013**, *24*, 1–7.
- (8) Cohoon, K. P.; Heit, J. A. *Clin. Chem.* **2013**, *59*, 1299–1300.
- (9) Lawson, J. H.; Murphy, M. P. *Semin. Hematol.* **2004**, *41*, 55–64.
- (10) Kroll, M. H. *Clin. Lab. News* **2010**, *36*, 8–10.
- (11) Bischof, D.; Dalbert, S.; Zollinger, A.; Ganter, M. T.; Hofer, C. K. *Minerva Anestesiol.* **2010**, *76*, 131–137.
- (12) CRASH-2 trial collaborators; Shakur, H.; Roberts, I.; Bautista, R.; Caballero, J.; Coats, T.; Dewan, Y.; El-Sayed, H.; Gogichaishvili, T.; Gupta, S.; Herrera, J.; Hunt, B.; Iribhogbe, P.; Izurieta, M.; Khamis, H.; Komolafe, E.; Marrero, M. A.; Mejia-Mantilla, J.; Miranda, J.; Morales, C.; Olaomi, O.; Olladashi, F.; Perel, P.; Peto, R.; Ramana, P. V.; Ravi, R. R.; Yutthakasemsunt, S. *Lancet* **2010**, *376*, 23–32.

- (13) Johansson, P. I.; Stensballe, J.; Oliveri, R.; Wade, C. E.; Ostrowski, S. R.; Holcomb, J. B. *Blood* **2014**, *124*, 3052–3058.
- (14) Anderson, L.; Quasim, I.; Soutar, R.; Steven, M.; Macfie, A.; Korte, W. *Transfus. Med.* **2006**, *16*, 31–39.
- (15) Tanaka, K. A.; Key, N. S.; Levy, J. H. *Anesth. Analg.* **2009**, *108*, 1433–1446.
- (16) Ferraris, V. A.; Ferraris, S. P.; Saha, S. P.; Hessel, E. A., II; Haan, C. K.; Royston, B. D.; Bridges, C. R.; Higgins, R. S.; Despotis, G.; Brown, J. R.; Spiess, B. D.; Shore-Lesserson, L.; Stafford-Smith, M.; Mazer, C. D.; Bennett-Guerrero, E.; Hill, S. E.; Body, S. *Ann. Thorac. Surg.* **2007**, *83*, S27–S86.
- (17) McMichael, M. A.; Smith, S. A. *Vet. Clin. Pathol.* **2011**, *40*, 140–153.
- (18) Park, M. S.; Martini, W. Z.; Dubick, M. A.; Salinas, J.; Butenash, S.; Kheirabadi, B. S.; Pusateri, A. E.; Vos, J. A.; Guymon, C. H.; Wolf, S. E.; Mann, K. G.; Holcomb, J. B. *J. Trauma* **2009**, *67*, 266–276.
- (19) Chitlur, M.; Sorensen, B.; Rivard, G. E.; Young, G.; Ingerslev, J.; Othman, M.; Nugent, D.; Kenet, G.; Escobar, M.; Lusher, J. *Haemophilia* **2011**, *17*, 532–537.
- (20) Evans, P. A.; Hawkins, K.; Williams, P. R. *Rheol. Rev.* **2006**, *255*–291.
- (21) Hayashi, Y.; Katsumoto, Y.; Omori, S.; Yasuda, A.; Asami, K.; Kaibara, M.; Uchimura, I. *Anal. Chem.* **2010**, *82*, 9769–9774.
- (22) Kaibara, M. *J. Biorheol.* **2009**, *23*, 2–10.
- (23) Debye, P. *Polar Molecules*; Chemical Catalog Co.: New York, 1929.
- (24) Grant, E. H.; Sheppard, R. J.; South, G. P. *Dielectric Behaviour of Biological Molecules in Solution*; Oxford University Press: Oxford, 1978.
- (25) Foster, K. R.; Schwan, H. P. *Crit. Rev. Biomed. Eng.* **1989**, *17*, 25–104.
- (26) Pethig, R. *Dielectric and Electronic Properties of Biological Materials*; John Wiley & Sons: New York, 1979.
- (27) Takashima, S. *Electrical Properties of Biopolymers and Membranes*; IOP Publishing Ltd: Philadelphia, 1989.
- (28) Asami, K. *Prog. Polym. Sci.* **2002**, *27*, 1617–1659.
- (29) Feldman, Y.; Ermolina, I.; Hayashi, Y. *IEEE Trans. Dielectr. Electr. Insul.* **2003**, *10*, 728–753.
- (30) Chiba, S.; Uchibori, K.; Fujiwara, T.; Ogata, T.; Yamauchi, S.; Shirai, T.; Masuo, M.; Okamoto, T.; Tateishi, T.; Furusawa, H.; Fujie, T.; Sakashita, H.; Tsuchiya, K.; Tamaoka, M.; Miyazaki, Y.; Inase, N.; Sumi, Y. *J. Sci. Res. Rep.* **2015**, *4*, 180–188.
- (31) Hayashi, Y.; Oshige, I.; Katsumoto, Y.; Omori, S.; Yasuda, A.; Asami, K. *Phys. Med. Biol.* **2008**, *53*, 2553–2564.
- (32) Irimajiri, A.; Ando, M.; Matsuoka, R.; Ichinowatari, T.; Takeuchi, S. *Biochim. Biophys. Acta, Gen. Subj.* **1996**, *1290*, 207–209.
- (33) Asami, K.; Sekine, K. *J. Phys. D: Appl. Phys.* **2007**, *40*, 2197–2204.
- (34) Cines, D. B.; Lebedeva, T.; Nagaswami, C.; Hayes, V.; Massefski, W.; Litvinov, R. I.; Rauova, L.; Lowery, T. J.; Weisel, J. *W. Blood* **2014**, *123*, 1596–1603.
- (35) Kasahara, K.; Kaneda, M.; Miki, T.; Iida, K.; Sekino-Suzuki, N.; Kawashima, I.; Suzuki, H.; Shimonaka, M.; Arai, M.; Ohno-Iwashita, Y.; Kojima, S.; Abe, M.; Kobayashi, T.; Okazaki, T.; Souris, M.; Ichinose, A.; Yamamoto, N. *Blood* **2013**, *122*, 3340–3348.
- (36) Bordi, F.; Cametti, C.; Gili, T. *Bioelectrochemistry* **2001**, *54*, 53–61.
- (37) Kremer, F.; Schönhals, A. *Broadband Dielectric Spectroscopy*; Springer: Berlin, 2003.
- (38) Chakroun, T.; Gerotzafas, G. T.; Seghatchian, J.; Samama, M. M.; Hatmi, M.; Elalamy, I. *Thromb. Haemost.* **2006**, *95*, 822–828.
- (39) Cooper, J. A. *J. Cell Biol.* **1987**, *105*, 1473–1478.
- (40) Cerecedo, D.; Stock, R.; González, S.; Reyes, E.; Mondragón, R. *Haematologica* **2002**, *87*, 1165–1176.
- (41) Laudano, A. P.; Doolittle, R. F. *Proc. Natl. Acad. Sci. U. S. A.* **1978**, *75*, 3085–3089.
- (42) Rijkers, D. T.; Wielders, S. J.; Béguin, S.; Hemker, H. C. *Thromb. Res.* **1998**, *89*, 161–169.
- (43) Dobbe, J. G.; Streekstra, G. J.; Strackee, J.; Rutten, M. C.; Stijnen, J. M.; Grimbergen, C. A. *IEEE Trans. Biomed. Eng.* **2003**, *50*, 97–106.
- (44) Fabry, T. L. *Blood* **1987**, *70*, 1572–1576.
- (45) Chernysh, I. N.; Weisel, J. W. *Blood* **2008**, *111*, 4854–4861.
- (46) Chernysh, I. N.; Nagaswami, C.; Weisel, J. W. *Blood* **2011**, *117*, 4609–4614.
- (47) Rand, M. D.; Lock, J. B.; van't Veer, C.; Gaffney, D. P.; Mann, K. G. *Blood* **1996**, *88*, 3432–3445.
- (48) Hunter, R. L.; Papadea, C.; Gallagher, C. J.; Finlayson, D. C.; Check, I. J. *Thromb. Haemost.* **1990**, *63*, 6–12.
- (49) van Gelder, J. M.; Nair, C. H.; Dhall, D. P. *Biorheology* **1994**, *31*, 259–275.
- (50) Ninivaggi, M.; Apitz-Castro, R.; Dargaud, Y.; de Laat, B.; Hemker, H. C.; Lindhout, T. *Clin. Chem.* **2012**, *58*, 1252–1259.